NUMERICAL-EXPERIMENTAL STUDY OF THE BOILING HEAT TRANSFER COEFFICIENT IN A THERMOSYPHON

Felipe Mercês BIGLIA[1], Victor Vaurek DIMBARRE[2], Guilherme Antonio BARTMEYER[2], Paulo Henrique DIAS DOS SANTOS[3], Thiago ANTONINI ALVES[1,2*]

[1]Federal University of Technology – Paraná, Curitiba/PR, Brasil

[2]Federal University of Technology – Paraná, Ponta Grossa/PR, Brasil

[3]Federal University of Paraíba, João Pessoa/PB, Brasil

[*] Corresponding author; E-mail: antonini@utfpr.edu.br

Thermosyphons are passive heat exchanger devices that use the latent heat of vaporization of a working fluid to intensify heat transfer. They consist of a metallic tube, passed through a vacuum process, and filled with a working fluid, and use the action of gravity to circulate the fluid internally. They are used to enhance heat transfer in many industrial areas, such as aerospace, electronics, and telecommunications, among others. In the literature, several studies are related to the subject under study, both experimental and numerical analyses. Still, there isn't validation of the results, especially when obtaining the boiling heat transfer coefficient. Thus, the main objective of the present work consists of determining an experimental test bench, from Dirichlet's Condition, varying an evaporator wall temperature (303.15, 313.15, and 323.15K) and water filling ratio (50 and 100% of the evaporator's volume) into stainless-steel thermosyphon, providing experimental data for validation of numerical simulations carried out using the Ansys® Fluent™ software. The comparison between numerical and experimental results demonstrated good agreement validating the numerical methodology.

Key words*: thermosyphon, boiling, experimental, numerical, CFD*

1. Introduction

Thermosyphons, or gravity-assisted heat pipes, are passive heat transfer devices with high thermal conductivity [1]. They are composed of an evacuated tube and filled with a working fluid, carrying energy in the form of heat between its ends from the latent heat of vaporization, related to the evaporation and condensation of the working fluid [2]. Thermosyphons are devices that transfer heat with high performance and have a broad range of applications in engineering [3]. In particular, they are widely used in many industrial fields such as electronics, telecommunications, aerospace, solar heating systems, among others [4-7].

These devices are composed of three regions with different functions in their operation, and they are illustrated schematically in Fig. 1 [8]. The lower region of the thermosyphons, called the evaporator, is the region that contains the working fluid. This region absorbs heat from a hot source, causing evaporation of the working fluid. The pressure inside the device is lower than the external pressure because it passes through a vacuum process. Therefore, the working fluid initiates the

evaporation process at saturation temperatures below the temperature that would occur in the condition of ambient pressure. When evaporating, the vapor of the working fluid, due to the pressure gradients, moves through the center of the thermosyphons until it reaches the upper region, called condenser. The condenser dissipates the heat absorbed in the evaporator and transported by steam to a cold source, and can be a cold fluid flow, for example, causing vapor condensation. Due to the action of gravity, the condensed fluid returns to the evaporator region by seeping through the walls of the thermosyphons, closing the thermodynamic cycle. Between the evaporator and the condenser is located the adiabatic section, a transitional section between these two regions, and it has the function to connect both sections and there is no heat exchange with the external environment, and may be absent depending on the application [9].

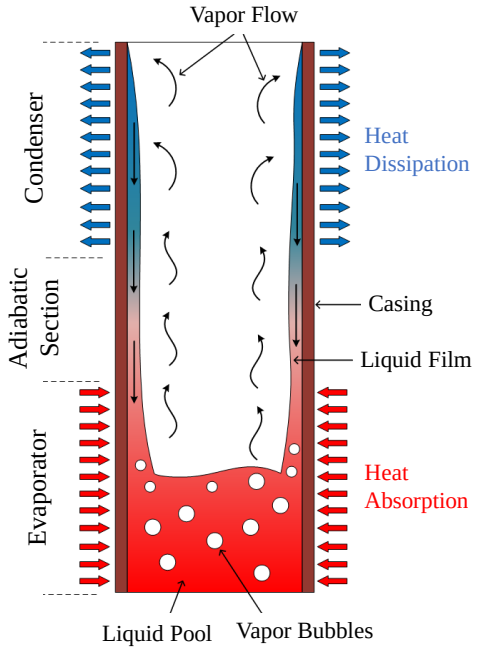

Figure 1. Thermosyphon's work principle [8]

In this context, the present work consists of the numerical-experimental study of the boiling heat transfer coefficient in a thermosyphon, varying the evaporator wall temperature (303.15, 313.15, and 323.15K) and the water filling ratio (50 and 100% of the evaporator's volume) in stainless steel thermosyphon in the bench test and afterwards, validated in numerical simulations carried out with the Ansys® Fluent™ software.

2. Experimental apparatus

A thermosyphon was constructed in a 304 stainless steel tube, with an outer diameter of 19.05mm, a wall thickness of 1.2mm and a total length of 1000mm, being 400mm for the evaporator, 200mm for the adiabatic section, and 400mm for the condenser. In the condenser was attached a cooling jacket, and it was constructed in 304 stainless steel tube with outer diameter of 38.10mm and the same length of condenser, as you can see in Fig. 2. To fill the thermosyphon, a Swagelok® needle valve was installed at its end. To take the temperatures, seven internal accesses (three equally spaced in the condenser, one in the adiabatic section, and three equally spaced in the evaporator) were installed to be connected to Omega Engineering® K-type pipe plug thermocouple probes. At the top of the thermosyphon an IFM® pressure transducer was installed for measuring the internal pressure.

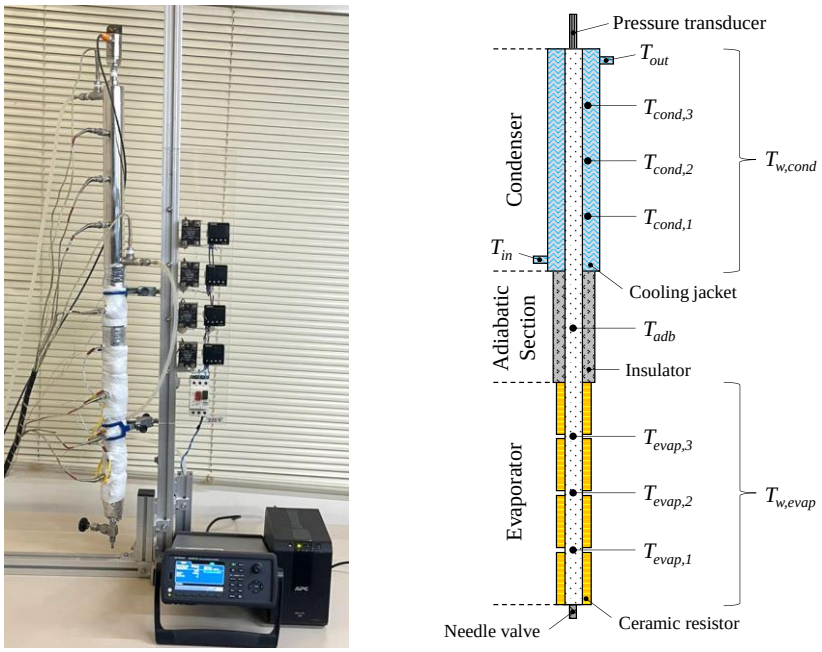

(a) apparatus (b) schematic diagram

Figure 2. Experimental apparatus

The experimental device used in this investigation was composed of a stainless steel thermosyphon, a Solab® ultrathermostatized bath, a Keysight® DAQ970A data acquisition system with a 20-channel multiplexer, a Dell® computer, and an APC® uninterruptible power supply. During the experimental tests, the evaporator was heated through the Joule effect, where there is electrical energy dissipation in four Omega Engineering® ceramic insulated band heaters with inner diameter of 19.05mm (3/4") and width of 101.6mm (4") and different evaporator wall temperatures were configured in Novus® PID controllers. For the cooling of the condenser, the ultrathermostatized bath provided a forced flow of water at a volumetric flow rate of 0.2L/min at a temperature of 291.15 ± 0.5K. The tests were conducted for a time of 7,000 seconds and the thermosyphon was maintained at an inclination of 90º with the horizontal (vertical position).

After the thermocouples were installed, a leakage test was performed, where compressed air was inserted to verify the sealing of the connections. This test is important to ensure that there is no leakage of working fluid or the air intake into the thermosyphon. After having passed the leakage test, the internal cleaning of the thermosyphon was performed and the evacuation procedure was performed. This procedure aims to remove all gases present inside the thermosyphon and thus reducing the internal pressure, for this it was connected to an EOS Value® vacuum pump, using Dow Corning® vacuum grease in the connections between the silicone hose, the pump and the valve.

Figure 3 shows a simplification of the experimental device with the objective of reproducing a physical model in a 2D Cartesian Coordinate System for numerical simulation using finite models, as will be presented in the subsequent topic.

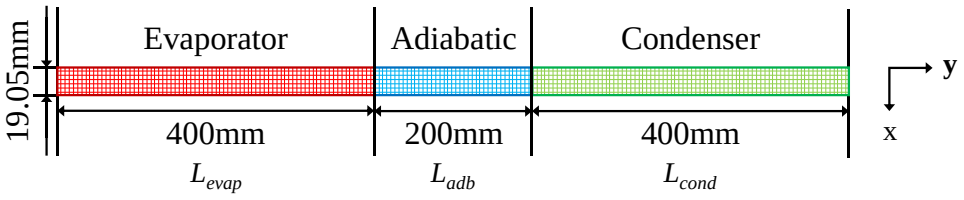

Figure 3. Model 2D

The experimental uncertainties related to the measurement instruments used are presented in Tab. 1.

Table 1. Experimental uncertainties

Parameter	Measuring Instrument	Uncertainty	Unit
Cooling Water	Ultrathermostatized bath	±0.5	K
Diameter	Caliper	±0.025	mm
Length	Millimeter scale	±0.5	mm
Pressure	Pressure Transducer	±2.0	kPa
Temperature	Type K thermocouple	±0.25	K

3. Model description

In this section will be addressed topics related to the simulation model to the solution and convergence criterion used in this work.

3.1. Simulation model

A Computational Fluid Dynamics (CFD) model was developed using Ansys® Fluent™ software, version 23 R2, two-phase flow was modeled using a Volume of Fluids (VOF) Model, using the Lee Model for evaporation and condensation. The saturation temperature was seated according the thermosyphon internal pressure data obtained from experimental tests, as shown in Tab. 2. The model constants used a value of $0.1s^{-1}$, for evaporation and condensation frequency, and it considered water as a working fluid, with filling ratios of 0.5 and 1.0 (the ratio of initial liquid volume per total evaporator's volume).

Table 2. Model properties acquired by experimental data

Filling ratio [%]	Evaporator Wall Temperature ($T_{w,evap}$) [K]	Pressure [kPa]	Saturation Temperature [K]
50	303.15	3.442	299.54
	313.15	5.266	306.95
	323.15	7.673	313.87
100	303.15	3.538	300.01
	313.15	4.185	302.89
	323.15	6.537	310.88

The governing equations for the VOF model to mass, momentum, and energy conservation are solved as presented in detail in [10,11]. Water liquid is defined as the primary (liquid) phase and water vapor is defined as the secondary (vapor) phase. During the evaporation and condensation processes, boiling temperatures were applied, according to the presented in Tab. 2.

The CFD modeled the details for two-phase flow and heat transfer phenomena under steady-state conditions found experimentally. Figure 4 illustrates the boundary conditions implemented in the computational model. This condition corresponds to a situation for which the surface is maintained at a fixed temperature. It is commonly called a Dirichlet condition, or a boundary condition of the first kind [12].

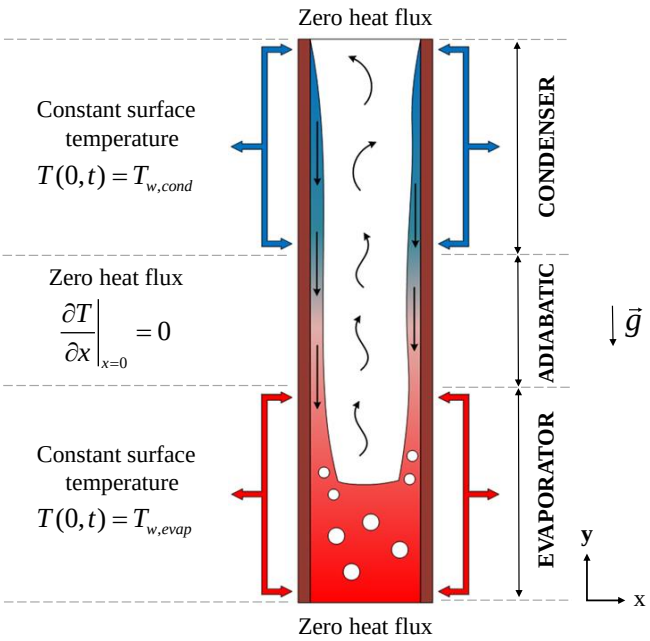

Figure 4. Boundary conditions of the thermosyphon

Details of the computational mesh used in the simulation of the thermosyphon is illustrated in Fig. 5. It is a uniform mesh that in its entirety has 367,294 nodes and 364,420 elements.

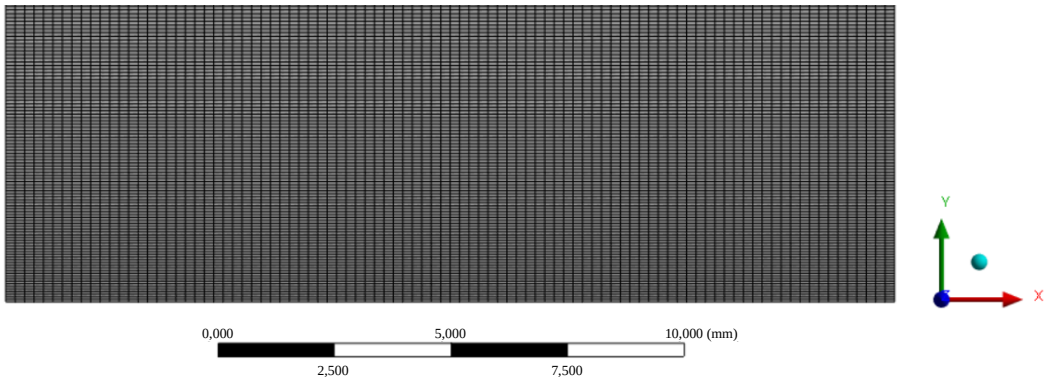

Figure 5. Details of a computational mesh section

3.2. Solution and convergence criterion

A transient simulation with a time step of 0.0005s was performed to model the dynamic behaviour of the two-phase flow. A combination of the SIMPLE Algorithm for pressure-velocity coupling and a Second-Order Upwind Scheme for the determination of momentum and energy is included in the model. Geo-Reconstruct and PRESTO discretization for the volume fraction and pressure interpolation scheme, respectively, are also performed in the simulation.

The numerical computation is considered to have converged when the scaled residual of the mass and velocity components is less than 10^{-5}. The computer used for the simulations has an Intel® Core™ i9-12900K 12th CPU @ 3.20GHz and 64GB of RAM.

3.3. Data reduction

The heat transfer rate, q, was calculated using the Joule's Law, through the product between the voltage and current applied at the ceramic resistance, which are positioned in the evaporator of the thermosyphon. The heat transfer coefficient was calculated using the Newton's Law of Cooling given by Eq. 1 [13].

$$h = \frac{q''}{\Delta T_e} = \frac{q}{\pi D L_{evap} \Delta T_e} \tag{1}$$

where q'' is the heat flux, L_{evap} is the evaporator length (where power dissipation occurs), and D is the diameter of the thermosyphon. $\Delta T_e \equiv T_{evap} - T_{sat}$, whereupon, T_{evap} corresponding to the evaporator temperature and T_{sat} corresponding to the saturation temperature of the water at the internal pressure of the thermosyphon.

4. Results

Figure 6 shows the temperature distribution versus time for each wall temperature applied at stainless steel thermosyphon. It can be seen that the highest temperatures are located in the evaporator region, where there is heat dissipation, and the lowest temperatures recorded are present in the condenser, where cooling is being carried out by the jacket through forced convection of water. These results demonstrate the expected behavior for a thermosyphon. Some variations in temperatures may be noted due to some phenomena internal to the device, such as the Geyser boiling effect [14], and instabilities due to the imbalance between the amount of condensed fluid and the evaporated fluid .

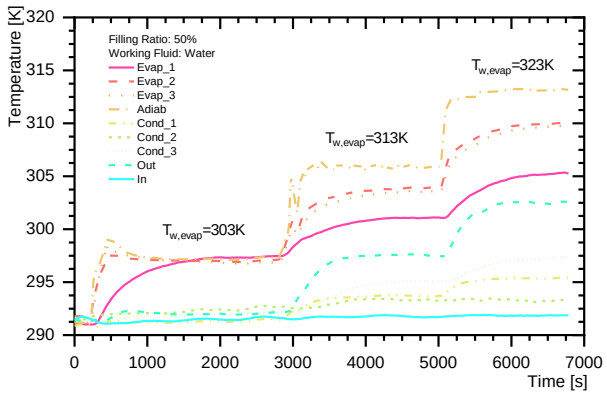

(a) FR 50%

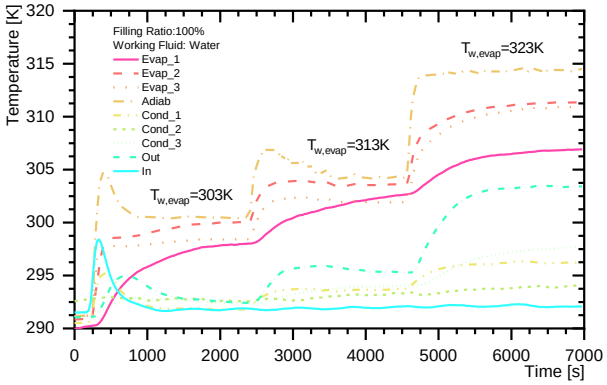

(b) FR 100%

Figure 6. Temperature distribution on the thermosyphon versus time at experimental test

Figure 7 presents the internal pressure versus time during the experimental test, and it can be seen, for every wall temperature applied the internal pressure increased. Since the internal pressure is proportional to the temperature values, the phase change process is conditioned to a constant temperature; such proportionality of variation is obtained.

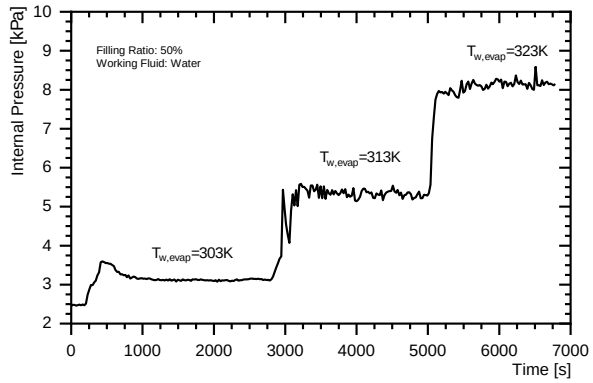

(a) FR 50%

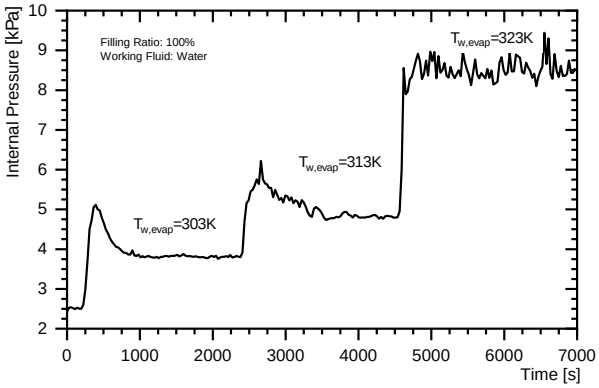

(b) FR 100%

Figure 7. Internal Pressure versus time at experimental test

The analysis of the pressure transducer data, including its uncertainty, reveals that the internal pressure values derived from the evaporator temperature fall within the defined error parameters, as illustrated in Fig. 8. Thus, it becomes reasonable considered that the internal pressure for each applied evaporator wall temperature can be calculated as a function of the internal evaporator temperature.

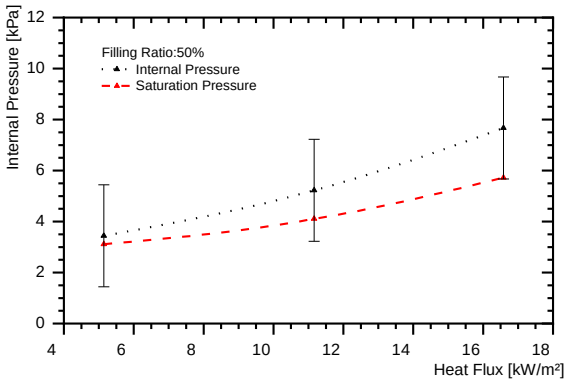

(a) FR 50%

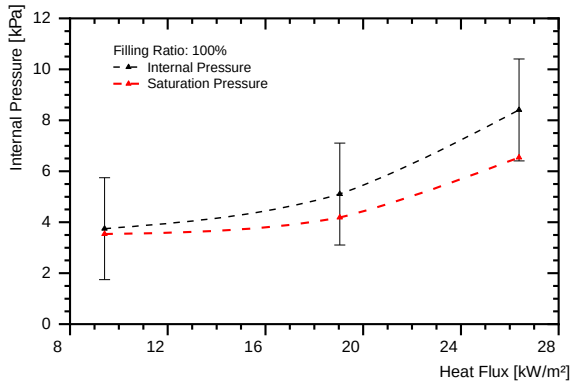

(b) FR 100%

Figure 8. Internal Pressure comparation versus heat flux

Figure 9 shows the behavior of the operating temperature (i.e., adiabatic section temperature) of the thermosyphon as a function of the evaporator wall temperature. It can be noted that such behavior was expected [15] since when supplying energy through electrical resistances, there is an increase in the temperature of the working fluid. To meet this information, it is possible to use the operating temperature to calculate the internal pressure during the application of thermal flux.

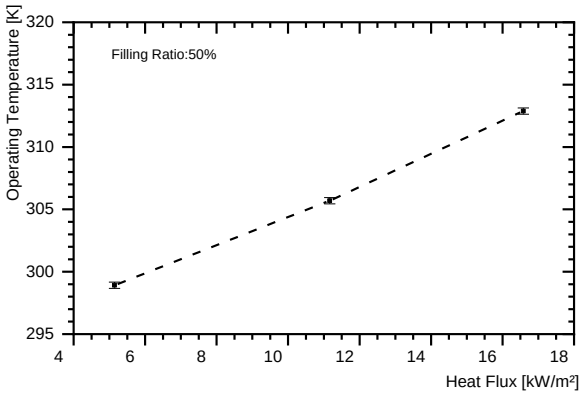

(a) FR 50%

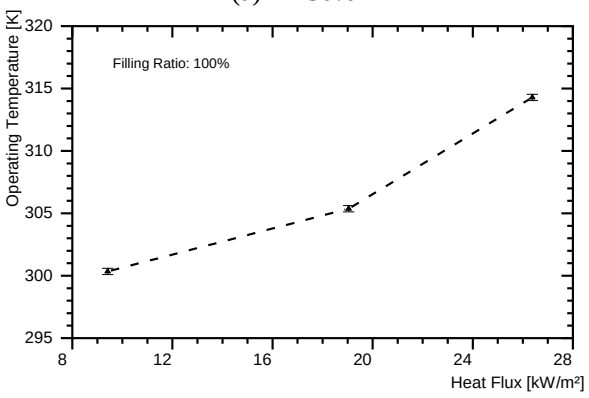

(b) FR 100%

Figure 9. Operating temperature depending on the heat flux applied

Figure 10 shows the relationship between the calculated internal pressure of the thermosyphon as a function of the applied thermal flux. It can be noted that, as presented in the literature [16], when providing a thermal load to the working fluid there is a change in its temperature and with this there is an increase in steam pressure, considering that the operating principle is based on biphasic exchange, so the internal pressure changes in response to variations in thermal load, maintaining constancy throughout the change process.

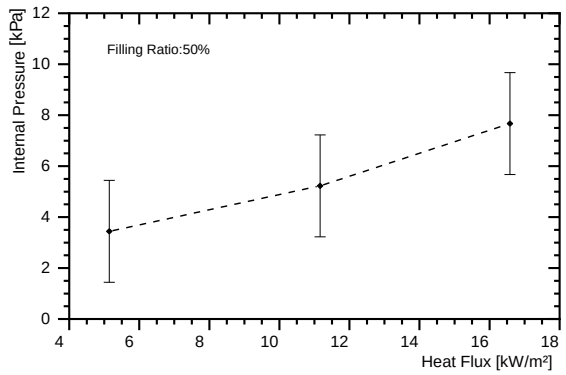

(a) FR 50%

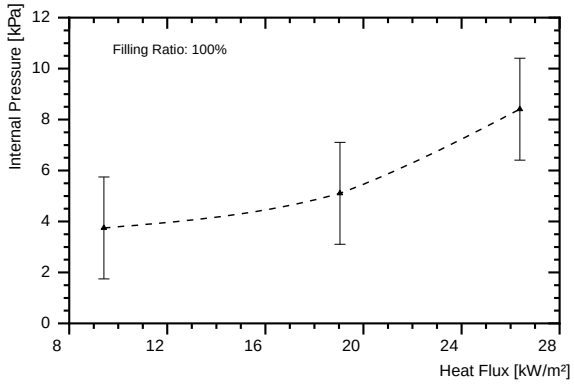

(b) FR 100%

Figure 10. Internal pressure depending on the heat flux applied

With the information of the experiment, Tab. 3 was constructed, which contains the boundary conditions for the numerical resolution of the problem in question.

Table 3. Boundary conditions of the numerical analysis

Evaporator		**Adiabatic**	**Condenser**
Filling ratio [%]	$T_{w,evap}$ **[K]**	q'' **[kW/m^2]**	$T_{w,cond}$ **[K]**
50	303.15	0	291.15
	313.15		
	323.15		
100	303.15		
	313.15		
	323.15		

Figure 11 presents the results for temperature distributions, via experimental and numerical solution, for each filling ratio. Figure 11(a) shows good agreement with the results and has the absolute and relative error values, 2.77K and 0.93%, respectively, for a wall temperature of 303.15K. Similarly, was observed in Fig. 11(b), the absolute and relative error values, 1.16K and 0.38%, respectively, for wall temperature of 303.15K.

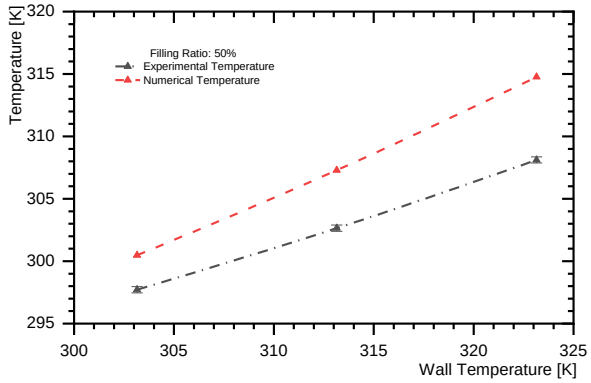

(a) FR 50%

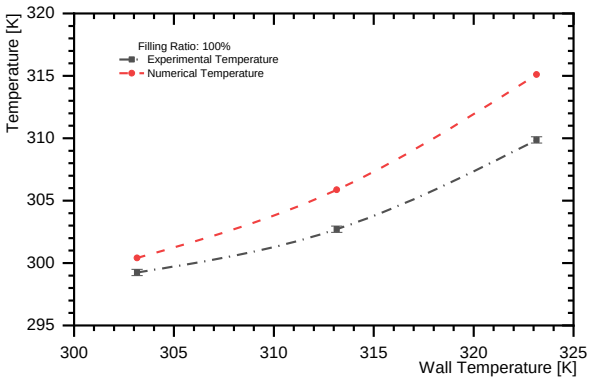

(b) FR 100%

Figure 11. Temperature distribution by wall temperature, filling ratio of (a) 0.5 and (b) 1.0

The application of Eq. (1) to obtain the boiling heat transfer coefficient depends on the values of saturation temperature, calculated as a function at the internal pressure of the thermosyphon, whose experimental errors do not allow its correct determination, therefore, numerical analysis is used to obtain it.

Table 4 presents the relative errors (R_{Error}) obtained through numerical and experimental analysis, relative to the heat flux. The high relative error rate is typical in heat transfer processes involving phase change due to the complexity and variability of the thermal conditions involved. This phenomenon introduces significant challenges to the accuracy of numerical models and experimental measurements, resulting in high discrepancies due to rapid transitions and variable thermal properties [14].

Table 4. Numerical-experimental analysis – heat flux

Filling ratio [%]	$T_{w,evap}$ **[K]**	q'' **[W/m^2]**	q''_{num} **[W/m^2]**	R_{Error} **[%]**
50	303.15	5,144	7,967	54.87
	313.15	11,164	20,358	82.35
	323.15	16,582	20,779	25.31
100	303.15	9,413	14,005	48.78
	313.15	19,045	33,453	75.66
	323.15	26,378	45,490	72.45

Table 5 presents the temperature results obtained using an *Ansys® Fluent™* software function of calculating the mean lengthave and location according to L_{evap} and boiling heat transfer coefficient of the numerical simulation performed in VOF.

Table 5. Numerical results - temperature and boiling heat transfer coefficient.

Filling ratio [%]	q''_{num} [W/m^2]	$T_{evap,num}$ [K]	h_{Num} [W/m^{2}K]
50	7,967	302.742	2,487
	20,358	312.379	3,750
	20,779	322.111	2,521
100	14,005	302.696	5,206
	33,453	312.110	3,630
	45,490	322.014	3,886

Figure 12 shows the volume fraction contours of pool boiling in the evaporator, with filling rates of 0.5 (Figs. 12(a), (c), and (e)) and 1.0 (Figs. 12(b), (d), and (f)), for evaporator wall temperature of 303.15, 313.15, and 323.15K. A red colour illustrates the presence of only vapour (vapour volume fraction = 1), while a blue colour stands for the presence of only liquid (vapour volume fraction = 0). At positions where the liquid reached the boiling temperature, the liquid starts to evaporate and phase change [17].

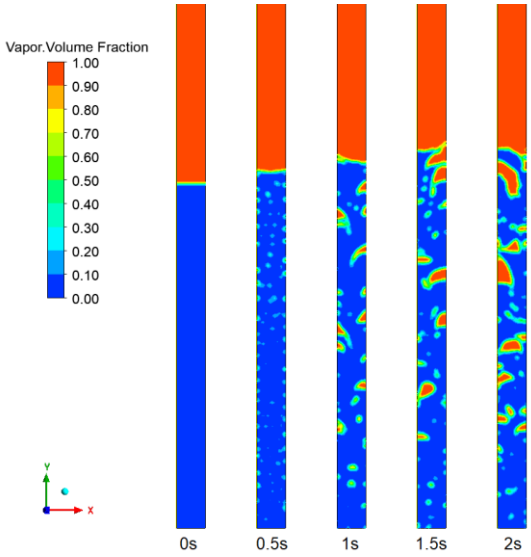

(a) 303.15K – FR 50%

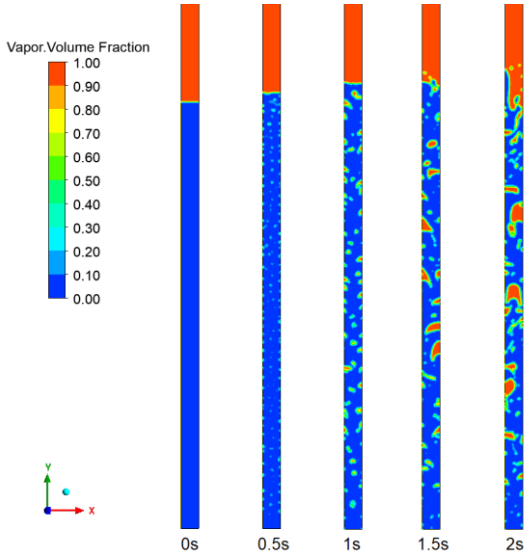

(b) 303.15K – FR 100%

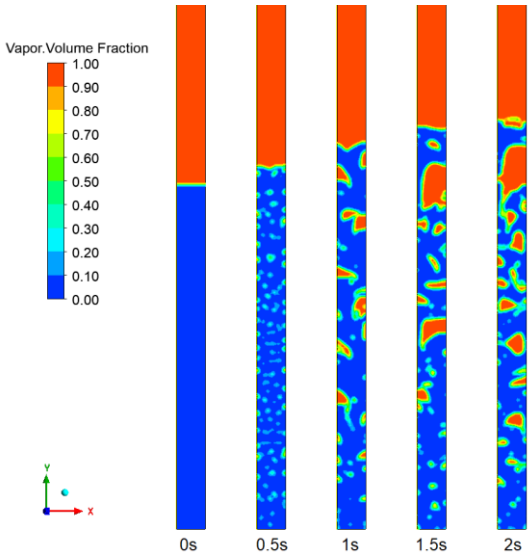

(c) 313.15K – FR 50%

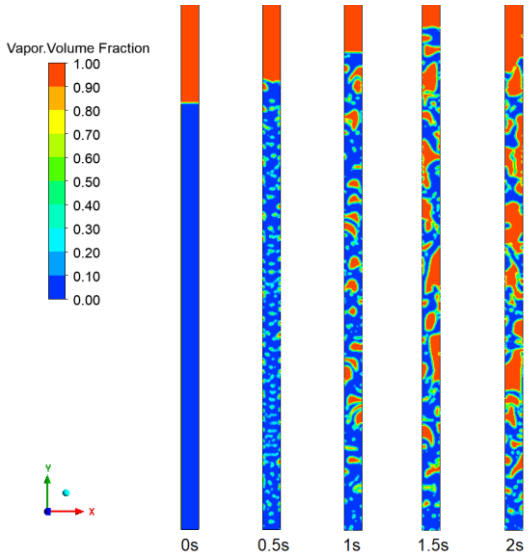

(d) 313.15K – FR 100%

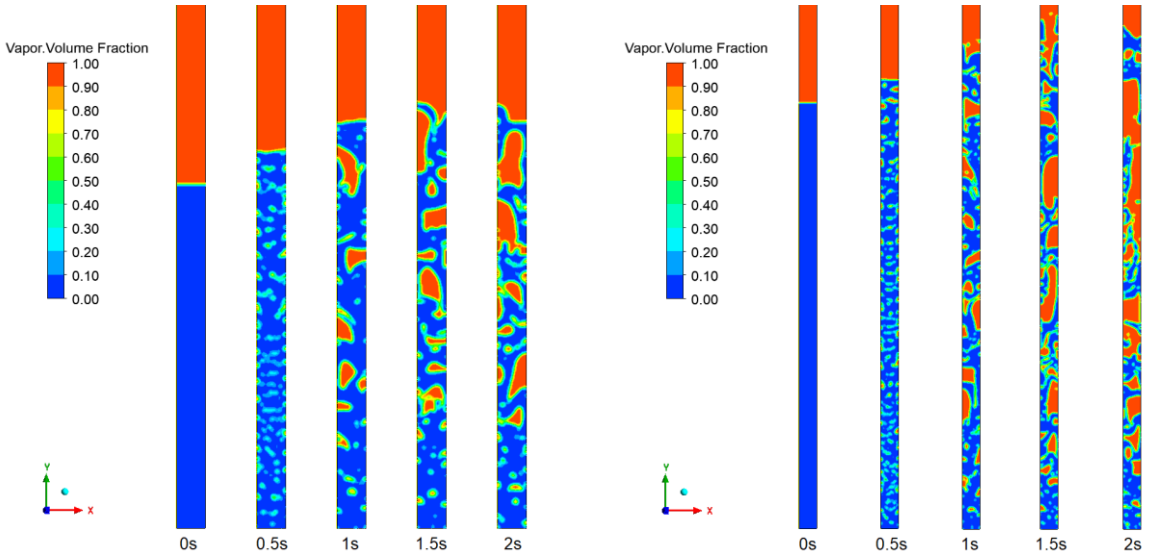

(e) 323.15K – FR 50% (f) 323.15K – FR 100%

Figure 12. Contours of volume fraction of pool boiling in the evaporator section at different *t* and *T*

5. CONCLUSION

The present work presented an experimental evaluation of the functioning of a thermosyphon manufactured in stainless steel using water as a working fluid and compared it to a numerical study using the VOF model in simulation. For the experiments, the evaporator was heated by the Joule effect, which consists of the dissipation of electrical power on the ceramic resistances present in the evaporator, the condenser cooling was made from a jacket that used water as cooling fluid. The analysis of the experimental results was based on the distribution of temperatures versus time and the evaluation of the internal pressure as a function of surface temperature in the evaporator. The simulation results showed that the high complexity phenomenon that occurs inside the thermosyphon can be modeled using the VOF method. The numerical results regarding the temperature present good agreement with the experimental ones, having the same behaviors and trends, thus allowing the assurance of a correct analysis of the phenomenon under study. The contribution of this work lies in the experimental and numerical evaluation of the performance of a stainless steel thermosyphon using water as the working fluid, comparing the results with a numerical study employing the VOF model. This study provides a significant advancement by demonstrating that the VOF method can accurately model complex phase change phenomena within the thermosyphon. However, further studies are necessary to explore different operational conditions and working fluids, as well as to refine the numerical models. This work aims to serve as a foundation for future investigations, contributing to the understanding and optimization of heat transfer processes in thermosyphons and developing more efficient designs for various applications.

Acknowledgment

The authors acknowledge the Capes, the CNPq, the PROPPG/UTFPR, the DIRPPG/ UTFPR, the PPGEM/UTFPR (Campus Ponta Grossa), and the DAMEC/ UTFPR (Campus Ponta Grossa). This research was funded by National Council for Scientific and Technologial Development (CNPq), grant numbers #409631/2021-3 and #312367/2022-8.

References

[1] Krambeck, L., Nishida, F. B., Aguiar, V. M., Santos, P. H. D., Antonini Alves, T., Thermal Performance Evaluation of Different Passive Devices for Electronic Cooling, *Thermal Science*, *23* (2019), 2B, pp. 1151-1160

[2] Jouhara, H., Reay, D. A., McGlen, R. J., Kew, P. A., McDonough, J., *Heat pipes: Theory, design and applications*, 7th ed. Butterworth-Heinemann, 2023.

[3] Nishida, F. B., Krambeck, L., Santos, P. H. D., Antonini Alves, T., Experimental Investigation of Heat Pipe Thermal Performance with Microgrooves Fabricated by Wire Electrical Discharge Machining (Wire-EDM), *Thermal Science*, *24* (2020), 2A, pp. 701-711

[4] Santos, P. H. D., Vicente, K. A. T., Reis, L. S., Marquardt, L. S., Antonini Alves, T., Modeling and Experimental Tests of a Copper Thermosyphon, *Acta Scientiarum. Technology (online)*, *39* (2017), 1, pp. 59-68

[5] Krambeck, L., Bartmeyer, G. A., Souza, D. O., Fusão, D., Santos, P. H. D., Antonini Alves, T., Experimental Thermal Performance of Different Capillary Structures for Heat Pipes, *Energy Engineering (Print)*, *118* (2021), 1, pp. 1-14

[6] Santos, P. H. D., Antonini Alves, T., Oliveira Junior, A. A. M., Bazzo, E., Analysis of a Flat Capillary Evaporator with a Bi-Layered Porous Wick, *Thermal Science*, *24* (2020), 3B, pp. 1951-1962

[7] Jafari, D., Franco, A., Filippeschi, S., Di Marco, P., Two-Phase Closed Thermosyphons: A Review of Studies and Solar Applications, *Renewable and Sustainable Energy Reviews*, *53* (2016), pp. 575-593

[8] Machado, P. L. O., Pereira, T. S., Trindade, M. G., Biglia, F. M., Santos, P. H. D., Tadano, Y. S., Siqueira, H., Antonini Alves, T., Estimating Thermal Performance of Thermosyphons by Artificial Neural Networks, *Alexandria Engineering Journal*, *79* (2023), pp. 93-104

[9] Mantelli, M. B. H., *Thermosyphons and heat pipes: Theory and applications*, 1st ed. Springer Nature, 2021

[10] Fadhl, B., Wrobel, L. C., Jouhara, H., Numerical Modelling of the Temperature Distribution in a Two-Phase Closed Thermosyphon, *Applied Thermal Engineering*, *60* (2013), pp. 122-131

[11] Jouhara, H., Fadhl, B., Wrobel, L. C., Three-Dimensional CFD Simulation of Geyser Boiling in a Two-Phase Closed Thermosyphon, *International Journal of Hydrogen Energy*, *41* (2016), pp. 16463-16476

[12] Faghri, A., Zhang, Y., *Fundamentals of multiphase heat transfer and flow*, 2nd ed. Springer Nature, 2020

[13] Bergman, T. L., Lavine, A. S., *Fundamentals of heat and mass transfer*, 8th ed. Wiley, 2018

[14] Souza, D. O., Machado, P. L. O., Chiarello, C., Santos, E. N., Silva, M. J., Santos, P. H. D., Antonini Alves, T., Experimental Study of Hydrodynamic Parameters Regarding on Geyser Boiling Phenomenon in Glass Thermosyphon using Wire-Mesh Sensor, *Thermal Science*, *26* (2022), 2B, pp. 1391-1404

[15] Krambeck, L., Bartmeyer, G. A., Souza, D. O., Fusão, D., Santos, P. H. D., Antonini Alves, T., Selecting Sintered Capillary Structure for Heat Pipes based on Experimental Thermal Performance, *Acta Scientiarum. Technology*, *44* (2022), e57099

[16] Santos, P. H. D., Krambeck, L., Santos, D. L. F., Antonini Alves, T., Analysis of a Stainless Steel Heat Pipe based on Operation Limits, *International Review of Mechanical Engineering*, *8* (2014), 3, pp. 599-608

[17] Shah, M. M., *Two-phase heat transfer*, 1st ed. Wiley, 2021

Paper submitted: 07 May 2024

Paper revised: 24 June 2024

Paper accepted: 26 June 2024